Joule

CellPress

Report

# Solid Acid Electrochemical Cell for the Production of Hydrogen from Ammonia

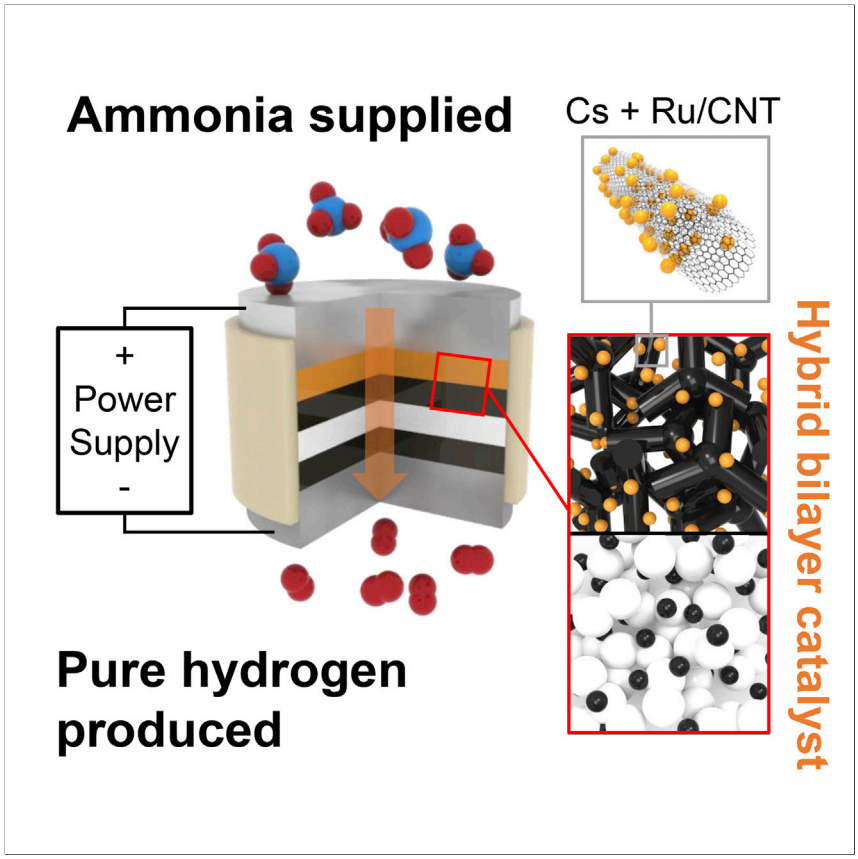


Ammonia has received increasing attention in recent years as an enabler of a sustainable energy future, in particular, as a carrier of hydrogen for use in fuel cells. Using superprotonic $CsH_2PO_4$ and a bilayer cathode structure, we show ammonia-to-hydrogen conversion with 100% faradic efficiency. Cs-promoted Ru serves as the ammonia decomposition catalyst, whereas Pt serves as the hydrogen electrooxidation catalyst and also as the hydrogen evolution catalyst at the anode. Zero ammonia crossover and zero side reactions result in an ultrahigh-purity product.

Dae-Kwang Lim, Austin B. Plymill, Haemin Paik, Xin Qian, Strahinja Zecevic, Calum R.I. Chisholm, Sossina M. Haile

sossina.haile@northwestern.edu

## HIGHLIGHTS

Superprotonic $CsH_2PO_4$ enables electrochemical cell operation at 250°C

Ammonia decomposition catalyst integrated with hydrogen electrooxidation catalyst

Ammonia converted to hydrogen with 100% faradic efficiency

Hydrogen production rate of 1.5 mol per gram catalyst per hour at 0.4 V bias

Lim et al., Joule 4, 2338–2347
November 18, 2020 
https://doi.org/10.1016/j.joule.2020.10.006

CellPress

Joule

Report

# Solid Acid Electrochemical Cell for the Production of Hydrogen from Ammonia

Dae-Kwang Lim,[1,4] Austin B. Plymill,[1,4] Haemin Paik,[1,2] Xin Qian,[1] Strahinja Zecevic,[3] Calum R.I. Chisholm,[3] and Sossina M. Haile[1,5,*]

## SUMMARY

**Production of high-purity hydrogen by thermal-electrochemical decomposition of ammonia at an intermediate temperature of 250°C is demonstrated. The process is enabled by use of a solid-acid-based electrochemical cell (SAEC) in combination with a bilayered anode, comprising a thermal-cracking catalyst layer and a hydrogen electrooxidation catalyst layer. Cs-promoted Ru on carbon nanotubes (Ru/CNT) serves as the thermal decomposition catalyst, and Pt on carbon black mixed with $CsH_2PO_4$ is used to catalyze hydrogen electrooxidation. Cells were operated at 250°C with humidified dilute ammonia supplied to the anode and humidified hydrogen supplied to the counter electrode. A current density of 435 mA/cm$^2$ was achieved at a potential of 0.4 V and ammonia flow rate of 30 sccm. With a demonstrated faradic efficiency for hydrogen production of 100%, the process yields hydrogen at a rate of 1.48 $mol_{H_2}/g_{cat}h$.**

## INTRODUCTION

Hydrogen has been proposed as an energy carrier in a sustainable energy future. When coupled with fuel cells, the energy content is converted on demand and with high efficiency into useful work, with water being the only emission generated at the point of use.[1] However, hydrogen has a low volumetric energy density, a low flash-point, and lacks a wide infrastructure for its storage and transport.[2–4] These challenges have led national governments to reconsider early commitments to hydrogen fuel cells.[5] Thus, realization of the potential environmental benefits of fuel cell technology is likely to rely on the identification of viable solutions to hydrogen storage and delivery. Ammonia has recently been suggested as an ideal candidate to act as a hydrogen vessel.[6–9] The molecule is lightweight, relatively much less flammable, easily liquefiable, commercially produced at high volume, and can make use of an existing delivery infrastructure.[10] Furthermore, although most ammonia production today utilizes hydrogen derived from natural gas and hence contributes to green-house gas emissions, cycling between stored hydrogen in ammonia and retrieved hydrogen can, in principle, be done without producing additional emissions.

The retrieval of hydrogen stored in ammonia is described by the decomposition reaction

$$NH_3 \rightarrow \frac{1}{2}N_2 + \frac{3}{2}H_2 \qquad \text{(Equation 1)}$$

This reaction is mildly endothermic at standard conditions with $\Delta_{rxn}H^0$ = 45.9 kJ/mol[11]; under standard pressure it proceeds spontaneously at temperatures

## Context & Scale

Ammonia has received increasing attention in recent years as a possible energy carrier, in particular, as a carrier of hydrogen for use in fuel cells. The traditional approach of thermal decomposition suffers from high concentrations of residual ammonia, which poison the catalysts in polymer electrolyte membrane fuel cells, whereas newer strategies based on electrochemical decomposition in aqueous solution operate at high overpotentials, implying low efficiency. Our approach integrates a thermal decomposition catalyst (Cs-promoted Ru on carbon nanotubes) with an all-solid-state electrochemical conversion cell (based on the proton-conducting electrolyte, $CsH_2PO_4$) in a device that is operable at 250°C. The resulting polarization curves indicate high current density at a modest voltage (far beyond what can be attained from alkali electrolyte cells), as well as catalyst utilization efficiency that far exceeds traditional thermal decomposition.

greater than 183°C. Achieving high conversion, however, requires high temperatures, typically beyond ~400°C, to overcome the twin challenges of thermodynamic limitations and kinetic barriers.[12] Residual ammonia in the fuel stream resulting from incomplete conversion is, in turn, highly detrimental to polymer electrolyte membrane fuel cells, the catalysts of which can tolerate no more than ~0.1 ppm $NH_3$.[13,14] As an alternative to high-temperature thermal decomposition, electrochemical decomposition of ammonia holds potential for production of high-purity hydrogen at near ambient conditions and with high conversion rates. To date, electrocatalytic approaches, which have largely employed aqueous alkali electrolytes, have required high operating potentials, implying poor energy efficiency, and have suffered from catalyst deactivation over time.[15,16] Accordingly, innovations in ammonia-to-hydrogen conversion are required if ammonia is to provide hydrogen on demand and serve as a flexible energy delivery medium.

Here, we pursue a hybrid thermal-electrochemical approach to the ammonia conversion reaction at an intermediate temperature of 250°C, with the aim of simultaneously addressing the $NH_3$ impurities in the hydrogen produced by high-temperature thermal decomposition and the low conversion efficiency of ambient temperature electrolysis. As the thermal decomposition catalyst, we employ Cs-promoted Ru on carbon nanotubes (Ru/CNT). This material is among the few catalysts to show substantial activity for ammonia decomposition at the low temperature of interest.[17–21] As the electrochemical component, we employ a cell based on the proton-conducting electrolyte, cesium dihydrogen phosphate (CDP), a solid acid compound that has long been exploited in intermediate temperature solid acid fuel cells (SAFCs)[22–29] and is non-reactive with $NH_3$ (Figure S1). The electrocatalyst is Pt, which has demonstrated high tolerance to fuel impurities at the operation temperature of 250°C (for example, up to 20% CO[22]), suggesting electrochemical functionality even in the presence of residual $NH_3$. By integrating the thermal decomposition with electrochemical removal of hydrogen from the reaction zone, we aim to overcome thermodynamic limitations otherwise imposed by product accumulation.

The overall configuration of the ammonia decomposition cells is presented in Figure 1. The internal thermal-cracking catalyst layer (TCL), Figures S2–S4, is placed adjacent to the hydrogen oxidation electrocatalyst layer (EL), which is, in turn, adjacent to the CDP electrolyte. The entire structure, which includes a hydrogen evolution electrocatalyst layer at the counter electrode, is placed between stainless steel mesh current collectors. The configuration is analogous to that used in direct methanol SAFCs[24] and other fuel cells operated on complex (non-hydrogen) fuels.[30]

## RESULTS AND DISCUSSION

Using three distinct cells to assess reproducibility, we first checked for leakage through the electrolyte membrane by measuring the open circuit voltage (OCV) with dilute $H_2$ supplied to the working electrode. The recorded voltages of 72, 73, and 73 mV were consistent with the value of 73 mV implied by the Nernst equation:

$$E_N = \frac{1}{2} RT \ln\left(\frac{p_{H_2}^{CE}}{p_{H_2}^{WE}}\right) \qquad \text{(Equation 2)}$$

where $R$ is the universal gas constant, $T$ is temperature, and $p_{H_2}^{WE}$ and $p_{H_2}^{CE}$ are the respective hydrogen partial pressures at the working and counter electrodes. The agreement between the Nernst and measured values demonstrates not only the absence of gas leaks but also the high ionic transference number of CDP. We then assessed the electrochemical characteristics under open circuit conditions by

[1]Department of Materials Science and Engineering, Northwestern University, 2220 Campus Drive, Evanston, IL 60208, USA

[2]Materials Science, California Institute of Technology, 1200 California Blvd., Pasadena, CA 91125, USA

[3]SAFCell Inc., 36 S. Chester Ave., Pasadena, CA 91106, USA

[4]These authors contributed equally

[5]Lead Contact

*Correspondence: sossina.haile@northwestern.edu

https://doi.org/10.1016/j.joule.2020.10.006

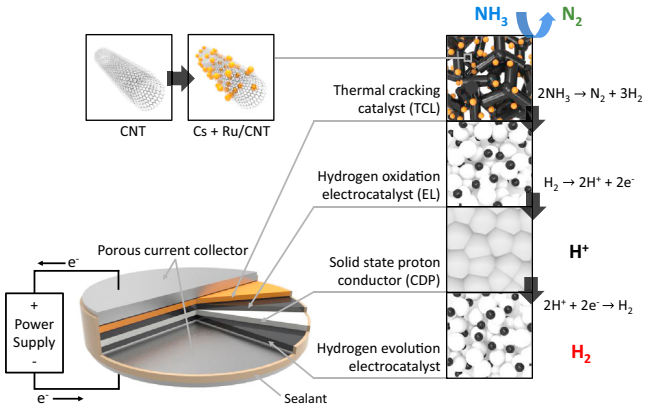


**Figure 1. Schematic of the Hybrid Thermal-Electrochemical Cell for On-Demand Ammonia-to-Hydrogen Conversion**

The thermal cracking layer (TCL) is adjacent to the hydrogen electrocatalyst layer (EL), which is, in turn, adjacent to a membrane of the solid-state proton conductor, CDP.

impedance spectroscopy, Figure S5. The measured ohmic losses of 0.24–0.26 $\Omega cm^2$ were comparable with the expected value of 0.25 $\Omega cm^2$ for the 50 μm-thick electrolyte with conductivity of 2.0 × $10^{-2}$ S/cm at 250°C.[23,31,32]

Polarization curves obtained under ammonia flow revealed excellent activity for ammonia decomposition, Figure 2A, as well as excellent cell-to-cell reproducibility, Table 1. The coincidence of the curves for the low $NH_3$ condition, measured before and after exposure to high $NH_3$, indicated good stability. A slight loss in performance, amounting to a 5%–6% decline in current density, could be due to the migration of the Cs promotor away from optimal sites in the Ru-Cs/CNT catalyst. Significantly, as expected for a solid-state electrolyte displaying pure protonic conduction, the faradic efficiency for hydrogen production was 100%, Figure 2B, and the generated hydrogen was free of impurities, Figure S6. Moreover, the data immediately revealed that substantially higher current densities were obtained upon supplying humidified $NH_3$ than dilute, humidified $H_2$, implying that electrochemical splitting of $H_2O$, which is in any case thermodynamically unfavorable, does not contribute to the observed currents. Accordingly, in Figure 2C the implied ammonia-to-hydrogen conversion rates are shown, which were computed from the ammonia supply rates in conjunction with the 100% faradic efficiency observation. The possibility of reaction of $NH_3$ with $H_2O$ during the ammonia oxidation reaction to form oxidized nitrogen (which would not impact the current efficiency for hydrogen production or hydrogen purity but would nevertheless be detrimental) was eliminated by chemical analysis of the anode side exhaust gas, Figure S7.

The voltages obtained under open circuit conditions were 78 ± 1 and 68 ± 4 mV (as averaged across the three cells), for the respective ammonia partial pressures of 0.4 and 0.6 atm. Inverting the Nernst relationship, these voltages imply hydrogen partial pressures at the working electrode of 0.019 and 0.033 atm, respectively. From this, we computed respective chemical ammonia-to-hydrogen conversion rates of 3.4% ± 0.1% and 3.5% ± 0.7% at the two ammonia concentrations. These values are generally in line with the results reported by Hill et al. (2%–10% conversion) for similar catalyst materials, with the precise value depending on Cs and Ru loadings.[17] Even for identical loadings, differences are expected due to differences in precursor types, deposition methods, CNT source, and gas flow conditions. The general

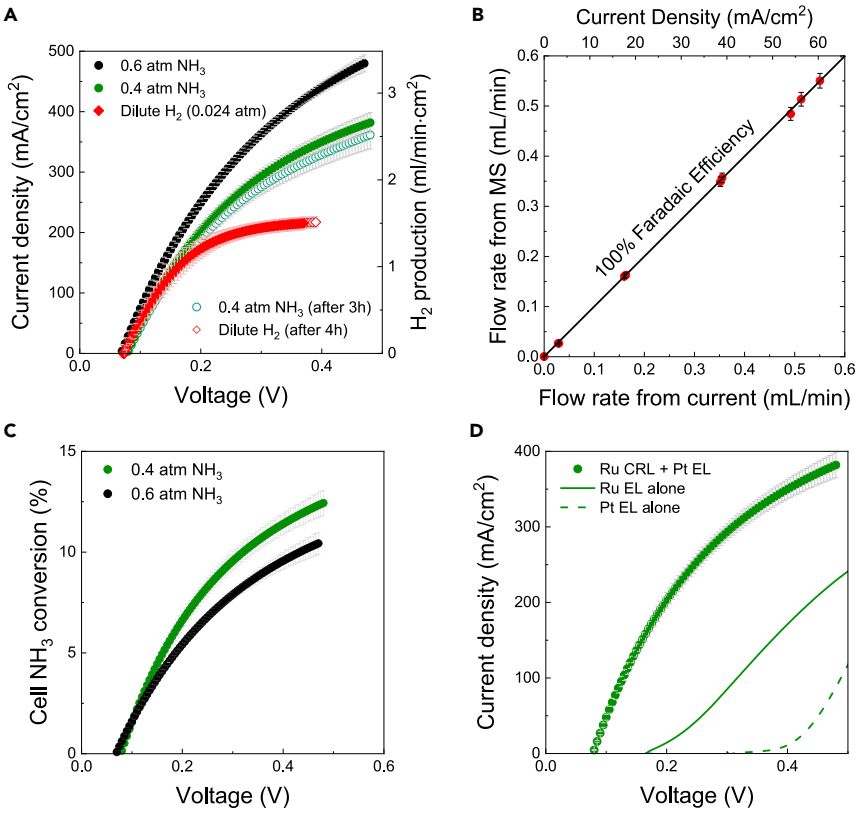


**Figure 2. Electrochemical Characteristics of Hybrid Thermal-Electrochemical Cells Designed for On-Demand Ammonia-to-Hydrogen Conversion**

(A) Polarization curves obtained upon supply of the gases indicated, along with computed $H_2$ production for 100% faradic efficiency.

(B) Measurement of $H_2$ evolved from cathode demonstrating 100% faradic efficiency.

(C and D) Implied $NH_3$ to $H_2$ conversion in (A) upon supply of the gases indicated (C); and comparison of polarization curves of bilayer electrode and single component electrodes, as indicated, under supply of 0.4 atm $pNH_3$ (D). Data of bilayer-electrode cells are the averages from three distinct cells. ($T$ = 250°C; supply to anode: 0.38 atm $pH_2O$, balance $N_2$; supply to cathode: 0.62 atm $pH_2$, balance $H_2O$). Error bars in (A), (C), and (D) are from averaging the data from these three cells. Error bars in (B) are from the uncertainty in the calibration of the mass spectrometer.

agreement between the results suggests that poisoning of Ru by $H_2O$, present in high concentration in this experiment and absent in Hill's work,[17] does not substantially interfere with ammonia decomposition at 250°C.

Away from open circuit conditions, the current rises under both ammonia and dilute hydrogen with a relatively low overall cell resistance, indicating rather moderate and similar overpotentials. Because the hydrogen partial pressures are similar between the three conditions ($pH_2$ = 0.024, 0.019, and 0.033 atm, respectively, in dilute hydrogen and at OCV in dilute and concentrated ammonia), the similarities in IV characteristics indicate that poisoning of the Pt electrocatalyst by unreacted $NH_3$ is negligible. This is further corroborated by the impedance results, which indicate similar electrochemical reaction resistance for the supply of dilute $H_2$ and of $NH_3$ under OCV conditions, Figure S5. These resistance values range from 0.16 to 0.19 $\Omega cm.^2$

With increasing current and voltage, the IV curves deviated from linearity and from one another. The concavity of the curves is suggestive of mass transport limitations

**Table 1. Summary of Electrical Characteristics of Three Independent Cells for Ammonia-to-Hydrogen Electrochemical Conversion**

| | At 0.4 $pNH_3$ | Current Density ($mA/cm^2$) at Voltage Indicated | | At 0.6 $pNH_3$ | Current Density ($mA/cm^2$) at Voltage Indicated | |
|---|---|---|---|---|---|---|
| Cell No. | OCV (V) | 0.15 V | 0.3 V | OCV (V) | 0.15 V | 0.3 V |
| 1 | 78 | 126 | 280 | 63 | 173 | 365 |
| 2 | 78 | 137 | 299 | 67 | 163 | 356 |
| 3 | 78 | 142 | 299 | 69 | 173 | 367 |
| Ave | 78 ± 1 | 135 ± 8 | 293 ± 11 | 68 ± 4 | 170 ± 6 | 363 ± 6 |

rather than Bulter-Volmer reaction kinetic limitations. In the case of dilute hydrogen, the IV curve plateaus relatively sharply at a current density corresponding to ~90% of the limiting value. This is consistent with the supposition that depletion of hydrogen is responsible for the declining rate of increase in cell current density and that $H_2O$ electrolysis does not occur under these conditions. Under ammonia, the IV curves followed a much more gradual change in slope. Moreover, the maximum current densities achieved (382 and 480 $mA/cm^2$ at low and high $pNH_3$, respectively) at the maximum measurement voltage of 0.47 V were only 12% and 10% of the respective limiting values. Based on the absence of any evidence of Pt poisoning, we conclude that the overall conversion process is limited by the characteristics of the TCL in the ammonia decomposition process. It is of some note that at these maximum conditions the hydrogen partial pressure at the cathode is estimated to increase from 0.62 to 0.65 atm, adding slightly to the measured voltage.

A further striking feature of the polarization curves, already alluded to above, is the substantially higher current densities achieved using 0.6 rather than 0.4 atm $pNH_3$. This behavior, which is consistent with electrochemical oxidation of ammonia being the source of the current, suggests that reactant depletion in the TCL can be compensated, at least in part, by increasing the reactant ($NH_3$) concentration. The resulting increase in current density, and hence the hydrogen production rate, was, however, accompanied by a decrease in conversion efficiency, Figure 2C. Thus, an increase in ammonia concentration did not result in a proportional increase in the availability of hydrogen. This observation points toward possible improvements by increasing the catalyst architecture to facilitate the removal of product $N_2$, or by increasing the thickness of the TCL to increase the residence time of $NH_3$ in the reaction zone, so long as this occurs without increasing the mass diffusion resistance. Beyond such design considerations, dramatic improvements may be possible by leveraging recent advances in TCL catalyst development.[18] Even in the absence of these steps, the polarization characteristics obtained here indicate performance characteristics that are far superior to those reported for alkali electrolysis cells in which large overpotentials (~0.4 V beyond the open circuit condition) must be overcome before non-negligible current flows.[15,16]

In the absence of the TCL, Figure 2D, the 20% Pt-C/CDP electrocatalyst displayed a relatively high OCV ~365 mV under $pNH_3$ of 0.4 atm, indicating negligible thermal ammonia decomposition ($< 1 \times 10^{-5}$ % conversion). The resulting currents under voltage bias were ~1% of the values obtained from the cells incorporating explicit thermal-cracking layers. From this, it can be concluded that, in the cells with distinct cracking and electrochemical catalyst layers, the Pt serves only to oxidize the hydrogen, at least up to 0.36 V, with the Ru-based catalyst accounting for almost the entirety of the $NH_3$ dissociation. On the other hand, in the absence of the Pt-based electrocatalyst, the cell with only the Ru/CNT + CDP dual-function catalyst

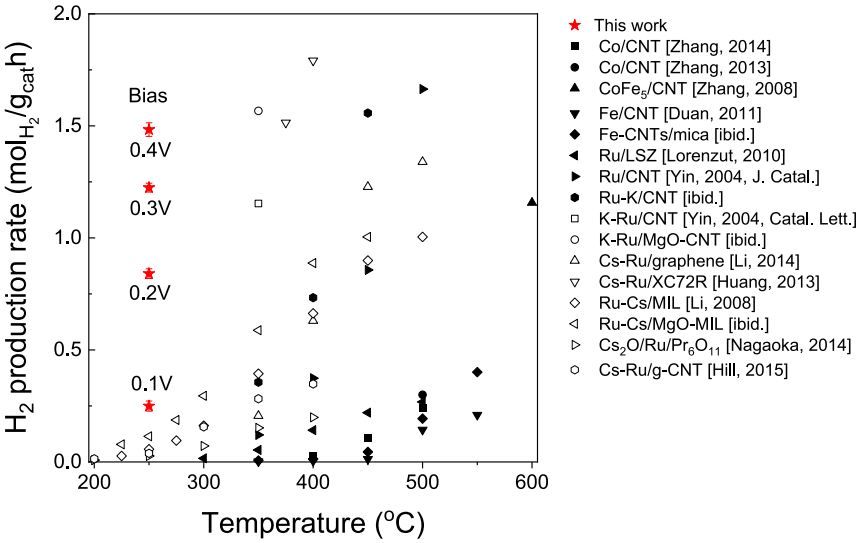


**Figure 3. Comparison, on a Catalyst-Mass Normalized Basis, of the Hydrogen Generation Rate Obtained from the Hybrid Thermal-Electrochemical Approach of this Work ($pNH_3$ = 0.6 atm) with Prior Work by Thermal Decomposition**

Literature data are taken from the sources cited in the figure.[18,19,33–42]

layer displayed surprisingly poor IV curves, Figure 2D. When 0.4 atm $pNH_3$ was supplied, the OCV was 170 mV (equivalent to 0.05% conversion), in contrast to 78 mV recorded from the bilayer-electrode system. The omission of the $CsNO_3$ promotor in this catalyst is likely the cause, as Ru is active for hydrogen electrooxidation under low current conditions (Figure S8). The result indicates that CDP is ineffective as a promotor, presumably because the phosphate anion is retained in the material at the temperatures of interest, preventing conversion to CsOH.

## Conclusion

It is shown here that, by integrating electrochemical product removal with thermal decomposition of ammonia, it is possible to generate hydrogen at a substantially higher rate than by thermal decomposition alone. To put these results into context, the hydrogen production rates achieved here were compared, on a catalyst-mass normalized basis, to those from conventional thermal-cracking experiments reported in the literature, Figure 3.[18,19,33–42] The hydrogen production rates were computed from the ammonia conversion and gas flow rates given in those publications. To fully account for the catalysts used in the present work, the catalyst in both the TCL and complete electrochemical cell were included in the normalization. From this representation, it is evident that the application of moderate bias (0.4 V) results in a catalyst-mass normalized hydrogen production rate that matches the results obtained from thermal decomposition at a much higher temperature of 350°C to 500°C. Furthermore, the evolved hydrogen is free of residual ammonia and the configuration is amenable to electrochemical compression of hydrogen, or to operation of a direct ammonia fuel cell without the risk of generating $NO_x$. A detailed efficiency analysis, which would require design of a system to minimize thermal inputs, is beyond the scope of this work, but a simple consideration of the minimum energy inputs relative to the energy content of the output hydrogen suggests high efficiencies are possible, Figure S9. In summary, the hybrid thermal-electrochemical approach demonstrated here, which integrates a solid-state proton conductor with an advanced thermal-cracking catalyst, shows great promise for ammonia-to-hydrogen or even ammonia-to-electricity conversion on demand.

## EXPERIMENTAL PROCEDURES

### Resource Availability

#### *Lead Contact*

Further information and requests for resources and materials should be directed to and will be fulfilled by the Lead Contact, Sossina Haile (sossina.haile@northwestern.edu).

#### *Materials Availability*

This study did not generate new, unique reagents.

#### *Data and Code Availability*

The published article includes all data analyzed during this study.

### CDP Stability Analysis

CDP powder was exposed to flowing humidified $NH_3$ ($pNH_3$ = 0.4 atm, $pH_2O$ = 0.38 atm, balance $N_2$) at a total gas flow rate of 50 sccm at 250°C for 24 h. During heating to the exposure condition, the gas supply was started after the sample reached a temperature of 150°C, and similarly on cooling, the gas supply was stopped at this temperature. Diffraction patterns collected before and after $NH_3$ exposure were identical, Figure S1.

### Synthesis

The catalyst for the TCL was prepared following the polyol method[43] in which ethylene glycol (Fisher Chemical, > 95% purity) served to reduce a metal salt precursor ($RuCl_3 \cdot 4.5H_2O$, Alfa Aesar, 99.9% metals basis). The Ru loading on the multi-walled CNTs (NanoLab, >95% purity) was fixed at 60 wt %, at which the ~30 nm diameter CNTs were fully coated with Ru nanoparticles, Figure S2. Cesium promotion was achieved by dispersing the Ru/CNT into a 50 mM aqueous solution of $CsNO_3$ (Alfa Aesar, 99.9%) with 1:1 molar ratio of Ru:Cs. The water was gently evaporated to induce precipitation of the nitrate. To promote uniformity the powder was dispersed in ethanol and the solvent evaporation repeated. Cells were fabricated using 53.4 mg of the Cs-promoted Ru/CNT material. The Ru crystallite size was 7 nm as determined by transmission electron microscopy imaging (Figure S2) and X-ray powder diffraction (Figure S3). On the basis of thermogravimetric analysis, it can be concluded that crystalline $CsNO_3$ obtained from the synthesis is decomposed to CsOH under $H_2$, in a reaction that is apparently catalyzed by metallic Ru (Figures S3 and S4).It is likely the decomposition process places CsOH in near proximity to the Ru, as suggested in the literature.[44,45]

### Cell Preparation

Three cells, 0.75″ in diameter, were fabricated and evaluated for ammonia decomposition. The EL was composed of Pt/carbon (20 wt % Pt on carbon black, HiSPEC® 3000, Alfa Aesar) and CDP (SAFCell) in a 1:6 mass ratio, as described in previous works (in which this component served as a hydrogen oxidation electrode).[28,46] For both TCL and EL components, 25 mg was used, resulting in respective Ru and Pt loadings of 10.3–11.1 and 0.5 mg/cm$^2$ over the active cell area of 1.34–1.45 cm$^2$. For ease of fabrication, a layer of carbon fiber paper (Toray, TGP-H-030) was placed between the two catalytic layers. The CDP electrolyte layer was 50 mg in mass and fully densified to yield a thickness of 50 μm. The hydrogen evolution (counter) electrode had the same formulation as the electrocatalyst in the working electrode and resulted in an additional 0.5 $mg_{Pt}/cm^2$ in the complete cell. For the purpose of assessing the role of individual components, two analogous additional cells were fabricated, the first in which the Ru-based TCL was omitted, and the

second in which the Pt-based EL was omitted. In the latter case, 60 wt % Ru/CNT, prepared as described above, was combined with CDP in a 1:6 mass ratio to serve as a direct ammonia oxidation electrocatalyst. Because of reactivity between CDP and most Cs salts, no additional promotor was applied.

### Electrochemical Measurements

Electrochemical measurements (BioLogic, SP-300) were performed at 250°C at a scan rate of 10 mV/s. Gas streams supplied to the anode and cathode were humidified (with steam partial pressure, $pH_2O$, of 0.38 atm) to prevent dehydration of the CDP electrolyte.[32,47,48] Humidified hydrogen ($pH_2$ = 0.62 atm) was supplied to the counter electrode, and either humidified ammonia at one of two concentrations ($pNH_3$ = 0.4 or 0.6 atm) or dilute-humidified hydrogen ($pH_2$ = 0.024 atm), balanced by a mixture of Ar and $N_2$, was supplied to the working electrode. The total gas flow rates at both electrodes was 50 sccm (standard cubic centimeters per minute) for all conditions. These flow rates imply limiting current densities for the 0.4 and 0.6 atm $NH_3$ fed cells of 3.0–3.2A/$cm^2$ and 4.5–4.8A/$cm^2$, respectively, based on the cell active areas and the hydrogen content of the supplied ammonia. Under supply of dilute $H_2$, the limiting currents are 247–267 mA/$cm^2$. faradic efficiency measurements were performed under similar conditions, but with humidified $N_2$ ($pH_2O$ = 0.38 atm) supplied to the counter electrode so as to ensure detection of only electrochemically evolved hydrogen and avoid drift of a high baseline in the mass spectrometer (Thermostar Pfeiffer GSD 301 T2) used for evolved gas chemical analysis.

## SUPPLEMENTAL INFORMATION

Supplemental Information can be found online at https://doi.org/10.1016/j.joule.2020.10.006.

## ACKNOWLEDGMENTS

The information, data, or work presented herein was funded in large part by the Advanced Research Projects Agency – Energy (ARPA-E), U.S. Department of Energy, under award number DE-AR0000813 of the REFUELS program. This work made use of the EPIC Facility of Northwestern University's NUANCE Center, which has received support from the Soft and Hybrid Nanotechnology Experimental (SHyNE) Resource (NSF ECCS-1542205); the MRSEC program (NSF DMR-1720139) at the Materials Research Center; the International Institute for Nanotechnology (IIN); the Keck Foundation; and the State of Illinois, through the IIN. Additionally, this work made use of the Jerome B. Cohen X-Ray Diffraction Facility supported by the MRSEC program of the National Science Foundation (DMR-1720139) at the Materials Research Center of Northwestern University. The views and opinions of authors expressed herein do not necessarily state or reflect those of the United States government or any agency thereof.

## AUTHOR CONTRIBUTIONS

C.R.I.C. and S.M.H. conceived the project, with S.M.H. providing overall supervision. D.-K.L., A.B.P., H.P., X.Q., and S.Z. designed and carried out experiments. D.-K.L., A.B.P., and S.M.H. analyzed the data. D.-K.L., A.B.P., H.P., S.Z., C.R.I.C., and S.M.H. added conceptual contributions. D.-K.L., A.B.P., H.P., C.R.I.C., and S.M.H. prepared and edited the manuscript.

## DECLARATION OF INTERESTS

D.-K.L., A.B.P., C.R.I.C., S.Z., and S.M.H. have filed the provisional US patent "solid acid electrochemical cells for the production of hydrogen from liquid fuels." C.R.I.C.

and S.Z. are employed by SAFCell, Inc., which aims to develop the technology described here. D.-K.L. is currently affiliated with the Korean Advanced Institute of Science and Technology, Yuseong-gu, Daejeon, Republic of Korea. H.P. is currently affiliated with the Massachusetts Institute of Technology, Cambridge, MA, USA.

Received: June 29, 2020
Revised: September 16, 2020
Accepted: October 8, 2020
Published: November 3, 2020

## REFERENCES

1. Edwards, P.P., Kuznetsov, V.L., David, W.I.F., and Brandon, N.P. (2008). Hydrogen and fuel cells: Towards a sustainable energy future. Energy Policy *36*, 4356–4362.

2. Markert, F., Marangon, A., Carcassi, M., and Duijm, N.J. (2017). Risk and sustainability analysis of complex hydrogen infrastructures. Int. J. Hydr. Energy *42*, 7698–7706.

3. Schlapbach, L., and Züttel, A. (2001). Hydrogen-storage materials for mobile applications. Nature *414*, 353–358.

4. Rivard, E., Trudeau, M., and Zaghib, K. (2019). Hydrogen storage for mobility: a review. Materials *12*.

5. Bullis, K. (2009). Q & A: energy secretary Steven Chu. MIT Technol. Rev.. https://www.technologyreview.com/2009/05/14/213138/q-a-steven-chu/

6. Soloveichik, G. (2016). Ammonia for energy storage and delivery. In 13th Annual NH3 Fuel Conference. https://nh3fuelassociation.org/events-conferences/conference2016/.

7. Klerke, A., Christensen, C.H., Nørskov, J.K., and Vegge, T. (2008). Ammonia for hydrogen storage: challenges and opportunities. J. Mater. Chem. *18*, 2304–2310.

8. Rouwenhorst, K.H.R., Van der Ham, A.G.J., Mul, G., and Kersten, S.R.A. (2019). Islanded ammonia power systems: technology review & conceptual process design. Renew. Sustain. Energy Rev. *114*, 109339.

9. Lamb, K.E., Dolan, M.D., and Kennedy, D.F. (2019). Ammonia for hydrogen storage; A review of catalytic ammonia decomposition and hydrogen separation and purification. Int. J. Hydr. Energy *44*, 3580–3593.

10. MacFarlane, D.R., Cherepanov, P.V., Choi, J., Suryanto, B.H.R., Hodgetts, R.Y., Bakker, J.M., Ferrero Vallana, F.M., and Simonov, A.N. (2020). A roadmap to the ammonia economy. Joule *4*, 1186–1205.

11. Chase, M.W. (1998). NIST-JANAF Thermochemical Tables (American Chemical Society; American Institute of Physics for the National Institute of Standards and Technology). https://webbook.nist.gov/cgi/cbook.cgi?Source=1998CHA1-1951&Units=SI&Mask=1.

12. Chiuta, S., Everson, R.C., Neomagus, H.W.J.P., van der Gryp, P., and Bessarabov, D.G. (2013). Reactor technology options for distributed hydrogen generation via ammonia decomposition: a review. Int. J. Hydr. Energy *38*, 14968–14991.

13. Uribe, F.A., Gottesfeld, S., and Zawodzinski, T.A. (2002). Effect of ammonia as potential fuel impurity on proton exchange membrane fuel cell performance. J. Electrochem. Soc. *149*, A293–A296.

14. Miyaoka, H., Miyaoka, H., Ichikawa, T., Ichikawa, T., and Kojima, Y. (2018). Highly purified hydrogen production from ammonia for PEM fuel cell. Int. J. Hydr. Energy *43*, 14486–14492.

15. Modisha, P., and Bessarabov, D. (2016). Electrocatalytic process for ammonia electrolysis: a remediation technique with hydrogen co-generation. Int. J. Electrochem. Sci. *11*, 6627–6635.

16. Vitse, F., Cooper, M., and Botte, G.G. (2005). On the use of ammonia electrolysis for hydrogen production. J. Power Sources *142*, 18–26.

17. Hill, A.K., and Torrente-Murciano, L. (2014). In-situ $H_2$ production via low temperature decomposition of ammonia: insights into the role of cesium as a promoter. Int. J. Hydr. Energy *39*, 7646–7654.

18. Hill, A.K., and Torrente-Murciano, L. (2015). Low temperature $H_2$ production from ammonia using ruthenium-based catalysts: synergetic effect of promoter and support. Appl. Cat. B *172–173*, 129–135.

19. Li, J.P., Wang, W.Y., Chen, W.X., Gong, Q.M., Luo, J., Lin, R.Q., Xin, H.L., Zhang, H., Wang, D.S., Peng, Q., et al. (2018). Sub-nm ruthenium cluster as an efficient and robust catalyst for decomposition and synthesis of ammonia: break the "size shackles. Nano Res. *11*, 4774–4785.

20. Mukherjee, S., Devaguptapu, S.V., Sviripa, A., Lund, C.R.F., and Wu, G. (2018). Low-temperature ammonia decomposition catalysts for hydrogen generation. Appl. Cat. B *226*, 162–181.

21. Yin, S.F., Xu, B.Q., Zhou, X.P., and Au, C.T. (2004). A mini-review on ammonia decomposition catalysts for on-site generation of hydrogen for fuel cell applications. Appl. Cat. A *277*, 1–9.

22. Chisholm, C.R.I., Boysen, D.A., Papandrew, A.B., Zecevic, S., Cha, S., Sasaki, K., Varga, A., Giapis, K.P., and Haile, S.M. (2009). From laboratory breakthrough to technological realization: the development path for solid acid fuel cells. Electrochem Soc Int. *18*, 53–59.

23. Haile, S.M., Chisholm, C.R.I., Sasaki, K., Boysen, D.A., and Uda, T. (2007). Solid acid proton conductors: from laboratory curiosities to fuel cell electrolytes. Faraday Discuss. *134*, 17–39.

24. Uda, T., Boysen, D.A., Chisholm, C.R.I., and Haile, S.M. (2006). Alcohol fuel cells at optimal temperatures. Electrochem. Solid-State Lett. *9*, A261–A264.

25. Uda, T., and Haile, S.M. (2005). Thin-membrane solid-acid fuel cell. Electrochem. Solid State Lett. *8*, A245–A246.

26. Boysen, D.A., Uda, T., Chisholm, C.R.I., and Haile, S.M. (2004). High-performance solid acid fuel cells through humidity stabilization. Science *303*, 68–70.

27. Otomo, J., Tamaki, T., Nishida, S., Wang, S.Q., Ogura, M., Kobayashi, T., Wen, C.J., Nagamoto, H., and Takahashi, H. (2005). Effect of water vapor on proton conduction of cesium dihydrogen phosphateand application to intermediate temperature fuel cells. J. Appl. Electrochem. *35*, 865–870.

28. Papandrew, A.B., Chisholm, C.R.I., Elgammal, R.A., Özer, M.M., and Zecevic, S.K. (2011). Advanced electrodes for solid acid fuel cells by platinum deposition on $CsH_2PO_4$. Chem. Mater. *23*, 1659–1667.

29. Scott, K., Xu, C.X., and Wu, X. (2014). Intermediate temperature proton-conducting membrane electrolytes for fuel cells. WIREs Energy Environ. *3*, 24–41.

30. Zhan, Z.L., and Barnett, S.A. (2005). An octane-fueled solid oxide fuel cell. Science *308*, 844–847.

31. Baranov, A.I., Khiznichenko, V.P., Sandler, V.A., and Shuvalov, L.A. (1988). Frequency dielectric dispersion in the ferroelectric and superionic phases of $CsH_2PO_4$. Ferroelectrics *81*, 183–186.

32. Otomo, J., Minagawa, N., Wen, C.J., Eguchi, K., and Takahashi, H. (2003). Protonic conduction of $CsH_2PO_4$ and its composite with silica in dry and humid atmospheres. Solid State Ionics *156*, 357–369.

33. Zhang, H., Alhamed, Y.A., Al-Zahrani, A., Daous, M., Inokawa, H., Kojima, Y., and Petrov, L.A. (2014). Tuning catalytic performances of cobalt catalysts for clean hydrogen generation via variation of the type of carbon support and catalyst post-treatment temperature. Int. J. Hydr. Energy *39*, 17573–17582.

34. Nagaoka, K., Eboshi, T., Abe, N., Miyahara, S., Honda, K., and Sato, K. (2014). Influence of

basic dopants on the activity of $Ru/Pr_6O_{11}$ for hydrogen production by ammonia decomposition. Int. J. Hydr. Energy *39*, 20731–20735.

35. Li, G., Nagasawa, H., Kanezashi, M., Yoshioka, T., and Tsuru, T. (2014). Graphene nanosheets supporting Ru nanoparticles with controlled nanoarchitectures form a high-performance catalyst for COx-free hydrogen production from ammonia. J. Mater. Chem. A *2*, 9185–9192.

36. Zhang, H., Alhamed, Y.A., Chu, W., Ye, Z.B., AlZahrani, A., and Petrov, L. (2013). Controlling Co-support interaction in Co/MWCNTs catalysts and catalytic performance for hydrogen production via $NH_3$ decomposition. Appl. Cat. A *464–465*, 156–164.

37. Huang, D.C., Jiang, C.H., Liu, F.J., Cheng, Y.C., Chen, Y.C., and Hsueh, K.L. (2013). Preparation of Ru-Cs catalyst and its application on hydrogen production by ammonia decomposition. Int. J. Hydr. Energy *38*, 3233–3240.

38. Duan, X.Z., Qian, G., Zhou, X.G., Sui, Z.J., Chen, D., and Yuan, W.K. (2011). Tuning the size and shape of Fe nanoparticles on carbon nanofibers for catalytic ammonia decomposition. Appl. Cat. B *101*, 189–196.

39. Lorenzut, B., Montini, T., Pavel, C.C., Comotti, M., Vizza, F., Bianchini, C., and Fornasiero, P. (2010). Embedded $Ru@ZrO_2$ catalysts for $H_2$ production by ammonia decomposition. ChemCatcChem *2*, 1096–1106.

40. Zhang, J., Müller, J.O., Zheng, W.Q., Wang, D., Su, D.S., and Schlögl, R. (2008). Individual Fe-Co alloy nanoparticles on carbon nanotubes: structural and catalytic properties. Nano Lett. *8*, 2738–2743.

41. Yin, S.F., Zhang, Q.H., Xu, B.Q., Zhu, W.X., Ng, C.F., and Au, C.T. (2004). Investigation on the catalysis of COx-free hydrogen generation from ammonia. J. Cat. *224*, 384–396.

42. Yin, S.F., Xu, B.Q., Wang, S.J., Ng, C.F., and Au, C.T. (2004). Magnesia-carbon nanotubes (MgO-CNTs) nanocomposite: novel support of Ru catalyst for the generation of COx-free hydrogen from ammonia. Cat. Lett. *96*, 113–116.

43. Kurihara, L.K., Chow, G.M., and Schoen, P.E. (1995). Nanocrystalline metallic powders and films produced by the polyol method. Nanostruct. Mater. *5*, 607–613.

44. Larichev, Y.V., Moroz, B.L., Zaikovskii, V.I., Yunusov, S.M., Kalyuzhnaya, E.S., Shur, V.B., and Bukhtiyarov, V.I. (2007). XPS and TEM studies on the role of the support and alkali promoter in Ru/MgO and Ru-Cs+/MgO catalysts for ammonia synthesis. J. Phys. Chem. C *111*, 9427–9436.

45. Aika, K.-i. (2017). Role of alkali promoter in ammonia synthesis over ruthenium catalysts—effect on reaction mechanism. Cat. Today *286*, 14–20.

46. Lim, D.K., Liu, J., Pandey, S.A., Paik, H., Chisholm, C.R.I., Hupp, J.T., and Haile, S.M. (2018). Atomic layer deposition of $Pt@CsH_2PO_4$ for the cathodes of solid acid fuel cells. Electrochim. Acta *288*, 12–19.

47. Ikeda, A., and Haile, S.M. (2012). The thermodynamics and kinetics of the dehydration of $CsH_2PO_4$ studied in the presence of $SiO_2$. Solid State Ionics *213*, 63–71.

48. Taninouchi, Y.K., Uda, T., Awakura, Y., Ikeda, A., and Haile, S.M. (2007). Dehydration behavior of the superprotonic conductor $CsH_2PO_4$ at moderate temperatures: 230 to 260 degrees C. J. Mater. Chem. *17*, 3182–3189.